J|A|C|S ARTICLES

Published on Web 11/05/2009

# Energy Transfer, Unfolding, and Fragmentation Dynamics in Collisions of N-Protonated Octaglycine with an H-SAM Surface

George L. Barnes and William L. Hase*

*Department of Chemistry and Biochemistry, Texas Tech University, Lubbock, Texas 79409*

Received June 24, 2009; E-mail: bill.hase@ttu.edu

***Abstract:*** Results are reported for PM3 and RM1 QM+MM direct dynamics simulations of collisions of N-protonated octaglycine ($gly_8$-$H^+$) with an octanethiol self-assembled monolayer (H-SAM) surface. Detailed analyses of the energy transfer, fragmentation, and conformational changes induced by the collisions are described. Extensive comparisons are made between the simulations and previously reported experimental studies. Good agreement between the two semiempirical methods is found regarding energy transfer, while differences are seen for their fragmentation time scales. Trajectories were calculated for 8 ps with collision energies from 5 to 110 eV and incident angles of 0° and 45°. A linear relationship is found between the collision energy and key parameters of the final internal energy distributions of both $gly_8$-$H^+$ and the H-SAM. In general wider distributions are seen for the H-SAM than for the peptide ion. An incident angle of 45° leads to more energy transfer to the peptide, with wider distributions. The average percentage energy transfer to $gly_8$-$H^+$ is nearly independent of the collision energy, while the average percentage transfer to the surface increases with collision energy. For normal incidence, we find an average percentage energy transfer to $gly_8$-$H^+$ which is in excellent agreement with the experimentally measured value 10.1 ± 0.8% for the octapeptide des-Arg$^1$-bradykinin [*J. Chem. Phys.* **2003**, *119*, 3414]. At each collision energy dramatic conformational changes of $gly_8$-$H^+$ are seen. The initial folded structure rearranges to form a $\beta$-sheet like structure showing that the collision induces peptide unfolding. This process is more pronounced at an incident angle of 45°. Following the conformation change, nonshattering fragmentation, promoted by proton transfer, is observed at the highest collision energies. Substantially more fragmentation occurs for the RM1 simulations.

## 1. Introduction

There is a broad interest in understanding the physical and chemical properties associated with collisions of protonated peptide ions with organic surfaces.[1−7] The two major physical processes occurring in these collisions, scattering and deposition of ions onto the surfaces, have been studied extensively by mass spectrometry.[1−12] An important scattering process is surface-induced dissociation (SID), in which a projectile fragments after colliding with a surface as a result of translation to vibration energy transfer. SID experiments provide a fast and relatively uncomplicated means of determining sequence information as the fragmentation patterns provide a "fingerprint" of the ion's structure. Both energetics[4,5,12,13] and reaction mechanics of fragmentation[13−16] can be determined through the coupling of SID and electrospray ionization. SID involving alkythiol self-assembled monolayers (H-SAM) and their fluorinated analogues (F-SAM) has been of particular interest.[2,4,12,14−28]

(1) Ouyang, Z.; Takáts, Z.; Blake, T. A.; Gologan, B.; Guymon, A. J.; Wiseman, J. M.; Oliver, J. C.; Davisson, V. J.; Cooks, R. G. *Science* **2003**, *301*, 1351–1354.
(2) Cooks, R. G.; Ast, T.; Pradeep, T.; Wysocki, V. *Acc. Chem. Res.* **1994**, *27*, 316–323.
(3) Miller, S. A.; Lou, H.; Pachuta, S. J.; Cooks, R. G. *Science* **1997**, *275*, 1447.
(4) Laskin, J.; Densiov, E.; Futrell, J. *J. Am. Chem. Soc.* **2000**, *122*, 9703.
(5) Wang, P.; Hadjar, O.; Gassman, P. L.; Laskin, J. *Phys. Chem. Chem. Phys.* **2008**, *10*, 1512.
(6) Laskin, J.; Wang, P.; Hadjar, O. *Phys. Chem. Chem. Phys.* **2008**, *10*, 1079.
(7) Barnes, G. L.; Hase, W. L. *J. Phys. Chem. A* **2009**, *113*, 7543–7547.
(8) Mabud, M. A.; Dekrey, M. J.; Cooks, R. G. *Int. J. Mass Spectrom. Ion Process.* **1985**, *67*, 285.
(9) McCormack, A. L.; Somogyi, Á.; Dongré, A. R.; Wysocki, V. H. *Anal. Chem.* **1993**, *65*, 2859.
(10) Burroughs, J. A.; Wainhaus, S. B.; Hanley, L. *J. Phys. Chem.* **1994**, *98*, 10913.
(11) Kubišta, J.; Dolejšek, Z.; Herman, Z. *Eur. J. Mass Spectrom.* **1998**, *4*, 311.
(12) Laskin, J.; Futrell, J. H. *J. Chem. Phys.* **2003**, *119*, 3413.
(13) Laskin, J. *J. Phys. Chem. A* **2006**, *110*, 8554.
(14) Laskin, J.; Bailey, T. H.; Futrell, J. H. *J. Am. Chem. Soc.* **2003**, *125*, 1625.
(15) Laskin, J.; Futrell, J. H. *J. Am. Soc. Mass Spectrom.* **2003**, *14*, 1340.
(16) Laskin, J.; Futrell, J. H. *Mass Spectrom. Rev.* **2003**, *22*, 158.
(17) Morris, M. R.; Riederer, J. D. E.; Winger, B. E.; Cooks, R. G.; Ast, T.; Chidsey, C. E. R. *Int. J. Mass Spectrom. Ion Process.* **1992**, *122*, 181.
(18) Pradeep, T.; Miller, S. A.; Cooks, R. G. *J. Am. Soc. Mass Spectrom.* **1993**, *4*, 769.
(19) Miller, S. A.; Riederer, J. D. E.; Cooks, R. G.; Cho, W. R.; Lee, H. W.; Kong, H. *J. Phys. Chem.* **1994**, *98*, 245.
(20) Pradeep, T.; Feng, B.; Ast, T.; Patrick, J. S.; Cooks, R. G.; Pachuta, S. J. *J. Am. Soc. Mass Spectrom.* **1995**, *6*, 187.
(21) Laskin, J.; Denisov, E.; Futrell, J. H. *J. Phys. Chem. B* **2001**, *105*, 1895.
(22) Laskin, J.; Futrell, J. H. *J. Chem. Phys.* **2002**, *116*, 4302.
(23) Jones, J. L.; Dongré, A. R.; Somogyi, Á.; Wysocki, V. H. *J. Am. Chem. Soc.* **1994**, *116*, 8368.

  

The two principal processes for ion deposition are "soft" and "reactive" landing. Soft-landing refers to the deposition of intact projectile ions onto the organic surface, including embedding into the bulk of the surface. Surfaces modified by soft-landing have a host of biological applications including development of microarrays,[1,29] novel biosensors,[30,31] and the characterization of molecular recognition at the fundamental amino acid level.[31] In reactive-landing the projectile is immobilized by covalent linkage with the surface. Surfaces with a broad range of functionality may be prepared by this technique;[5,32] e.g. conformationally selected α-helical peptide microarrays which may be used to characterize biological motifs by molecular recognition.[33]

Substantial progress has been made in the simulation of collisions of peptide-$H^+$ ions with surfaces.[7,34−45] Through the use of chemical dynamics simulations, energy transfer and fragmentation have been investigated in SID. Overall excellent agreement has been found between the simulations and experimental studies.[35,37,42] A strength of the simulations is that they provide an atomic-level understanding of the energy transfer and fragmentation dynamics. A diverse set of systems has been simulated, including $Si(CH_3)_3^+$, $Cr^+(CO)_6$, protonated polyglycine ($gly_n$-$H^+$), and polyalanine ($ala_n$-$H^+$) colliding with diamond {111}, alkylthiol self-assembled monolayer (H-SAM), and perfluorinated alkylthiol self-assembled monolayer (F-SAM) surfaces. The simulations have been performed using molecular mechanical (MM) functions for all of the potential energy terms and also QM+MM direct dynamics with the AM1 semiempirical[46] and MP2/6-31G(d)[36] methods used to represent the peptide-$H^+$ intramolecular potential. It has been shown that the percentage energy transfer to the colliding peptide is nearly independent of its size, and therefore the collision events have been thought of as being in the impulsive regime.[35,39,45] The identity of the surface is key to the final outcome. Surfaces such as diamond and the F-SAM have higher-energy transfer efficiencies, while surfaces such as the H-SAM have lower efficiencies.[12,35,39,45] SID is more efficient for the former surfaces, though fragmentation is also seen for the H-SAM at higher collision energies.[12] Studies of H- and F-SAMs therefore allow for investigation of the SID dynamics for different energy transfer efficiencies to the peptide. Fragmentation as the ion collides with the surface (i.e., shattering) is observed in simulations[34,36,40,41,46] and inferred for experiments.[14−16]

In this work we examine collisions between $gly_8$-$H^+$ and an octanethiol H-SAM surface using QM+MM direct dynamics simulations, with the potential energy of $gly_8$-$H^+$ represented by both the PM3[47] and RM1[48] semiempirical electronic structure theories. In the absence of electronic transitions the initial kinetic energy, $E_i$, is partitioned between final translational energy, $E_f$, the changes in internal energy of the peptide, $\Delta E_{peptide}$, and the surface, $\Delta E_{surf}$. Due to conservation of energy one can write

$$E_i = \Delta E_{peptide} + \Delta E_{surf} + E_f \quad (1)$$

A detailed analysis of the resulting energy distributions for both $gly_8$-$H^+$ and the H-SAM are described.

The results are compared with the experimental work of Laskin and Futrell[12] in which they collided the octa-peptide ion des-$Arg^1$-bradykinin with several surfaces including an H-SAM. Although their peptide is significantly larger than $gly_8$-$H^+$ we believe that this is unimportant since, as described above, the collisions are thought to be in the impulsive regime. In contrast to energy transfer, the fragmentation dynamics for $gly_8$-$H^+$ may differ from those for des-$Arg^1$-bradykinin. Laskin and Futrell provide a detailed analysis of the change in internal energy of des-$Arg^1$-bradykinin, including both the mean energy transfer as well as the full width at half-maximum (fwhm) of the distributions, which allows for a precise comparison with our computational results. The current work is also compared with previous simulations of peptide-$H^+$ collisions with an H-SAM,[42] as well as with other surfaces.

Conformational changes which take place during the collision are also examined. Such conformational changes can be thought of as the low energy/short time analogue of fragmentation. For the soft H-SAM such rearrangements are more likely since the fragmentation efficiency is smaller. Fragmentation occurs after the conformational changes and is only observed in the simulations for large collision energies. It is substantially more important when using the RM1 semiempirical method instead of PM3. Sufficient energy is transferred to $gly_8$-$H^+$ for fragmentation to occur at lower collision energies, but it does not on the 8 ps time scale of the simulations.

The outline of this paper is as follows. Section 2 describes the treatment of the potential and simulation methodology. The results are described and analyzed in section 3, comparisons to previous studies are made in section 4, and a summary is provided in section 5.

(24) Cooks, R. G.; Ast, T.; Mabud, M. A. *Int. J. Mass Spectrom. Ion Process.* **1990**, *100*, 209.
(25) Bier, M. E.; Schwartz, J. C.; Schey, K. L.; Cooks, R. G. *Int. J. Mass Spectrom. Ion Process.* **1990**, *103*, 1.
(26) Wright, A. D.; Despeyroux, D.; Jennings, K. R.; Evans, S.; Riddoch, A. *Org. Mass Spectrom.* **1992**, *27*, 525.
(27) Meot-Ner, M.; Dongré, A. R.; Somogyi, Á.; Wysocki, V. H. *Rapid Commun. Mass Spectrom.* **1995**, *9*, 829.
(28) Schey, K. L.; Durkin, D. A.; Thornburg, K. R. *J. Am. Soc. Mass Spectrom.* **1995**, *6*, 257.
(29) Gologan, B.; Takats, Z.; Alvarez, J.; Wiseman, J. M.; Talaty, N.; Ouyang, Z.; Cooks, R. G. *J. Am. Soc. Mass Spectrom.* **2004**, *15*, 1874.
(30) Love, J. C.; Estroff, L. A.; Kriebel, J. K.; Nuzzo, R. G.; Whitesides, G. M. *Chem. Rev.* **2005**, *105*, 1103–1169.
(31) Reimer, U.; Reineke, U.; Schneider-Mergener, J. *Curr. Opin. Biotechnol.* **2002**, *13*, 315–320.
(32) Wang, P.; Hadjar, O.; Laskin, J. *J. Am. Chem. Soc.* **2007**, *129*, 8682.
(33) Wang, P.; Laskin, J. *Angew. Chem., Int. Ed.* **2008**, *47*, 6678–6680.
(34) Park, K.; Deb, B.; Song, K.; Hase, W. L. *J. Am. Soc. Mass Spectrom.* **2009**, *20*, 939–948.
(35) Yang, L.; Mazyar, O. A.; Lourderaj, U.; Wang, J.; Rodgers, M. T.; Martínez-Núñez, E.; Addepalli, S. V.; Hase, W. L. *J. Phys. Chem. C* **2008**, *112*, 9377–9386.
(36) Park, K.; Song, K.; Hase, W. L. *Int. J. Mass Spectrom.* **2007**, *265*, 326.
(37) Rahaman, A.; Zhou, J. B.; Hase, W. L. *Int. J. Mass Spectrom.* **2006**, *249*, 321.
(38) Rahaman, A.; Collins, O.; Scott, C.; Wang, J.; Hase, W. L. *J. Phys. Chem. A* **2006**, *110*, 8418.
(39) Wang, J.; Meroueh, S. O.; Wang, Y.; Hase, W. L. *Int. J. Mass Spectrom.* **2003**, *230*, 57.
(40) Wang, Y.; Hase, W. L.; Song, K. *J. Am. Soc. Mass Spectrom.* **2003**, *14*, 1402.
(41) Song, K.; Meroueh, O.; Hase, W. L. *J. Chem. Phys.* **2003**, *118*, 2893.
(42) Meroueh, O.; Hase, W. L. *J. Am. Chem. Soc.* **2002**, *124*, 1524.
(43) Meroueh, O.; Hase, W. L. *Phys. Chem. Chem. Phys.* **2001**, *3*, 2306.
(44) Bosio, S. B. M.; Hase, W. L. *Int. J. Mass Spectrom. Ion Process.* **1998**, *174*, 1.
(45) Schultz, D. G.; Wainhaus, S. B.; Hanley, L.; de Sainte Claire, P.; Hase, W. L. *J. Chem. Phys.* **1997**, *106*, 10337.
(46) Meroueh, S. O.; Wang, Y.; Hase, W. L. *J. Phys. Chem. A* **2002**, *106*, 9983.
(47) Stewart, J. J. P. *J. Comput. Chem.* **1989**, *10*, 209.
(48) Rocha, G. B.; Freire, R. O.; Simas, A. M.; Stewart, J. J. P. *J. Comput. Chem.* **2005**, *27*, 1101–1111.

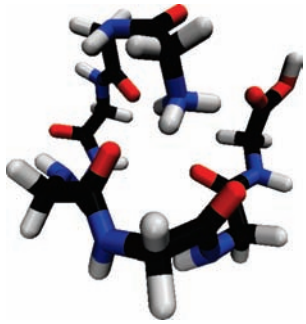

***Figure 1.*** Initial, folded structure of $gly_8$-$H^+$ optimized with PM3. This structure is stabilized by hydrogen bonding. The RM1 structure is similar, though slightly less spherical.

## 2. Computational Details

Our computational approach to simulating the $gly_8$-$H^+$ + H-SAM collision system begins with our definition of the global potential energy function as

$$V = V_{\text{peptide}} + V_{\text{surf}} + V_{\text{inter}} \tag{2}$$

where $V_{\text{peptide}}$ is the $gly_8$-$H^+$ intramolecular potential, $V_{\text{surf}}$ is the potential for the H-SAM, and $V_{\text{inter}}$ is the intermolecular interaction between the two. The $gly_8$-$H^+$ intramolecular potential is given by either the PM3 or RM1 semiempirical quantum mechanical (QM) method, while the other two terms are represented by molecular mechanical (MM) force fields. The resulting QM+MM potential is calculated on the fly for direct dynamics trajectory simulations.[49,50] Details of the potential and trajectories are discussed below. With the use of a QM model for $V_{\text{peptide}}$ the unimolecular dynamics of collisionally energized $gly_8$-$H^+$ may be studied, including proton transfer and fragmentation. Comparisons between the PM3 and RM1 methods indicate that RM1 is expected to give more accurate barrier heights and reaction enthalpies for organic and biochemical reactions.[48]

**2.1. Potential and Structure.** The use of semiempirical methods in MD simulations of protonated peptides has been shown to agree quite favorably with simulations treating the QM peptide with higher level MP2 methods.[36,40,46] The semiempirical approach has the great advantage of being computationally inexpensive which is essential as there are 60 QM atoms in the $gly_8$-$H^+$ + H-SAM system. The optimized PM3 geometry of $gly_8$-$H^+$ is shown in Figure 1. This structure was obtained by reoptimizing the structure used by Park et al.,[34] and is fairly spherical as is expected from the work of Hudgins and Jarrold.[51] The PM3 and RM1 structures differ in that the RM1 structure is slightly squished, though still fairly spherical and folded. The folded structures are stabilized by two intramolecular hydrogen bonds.

During the collision events an unfolding of the $gly_8$-$H^+$ structure is observed and it is therefore important to be able to quickly characterize the conformational state for each trajectory. To this end, the radius of gyration, $r_g$, and the asymmetry parameter, $\kappa$,[52] are used. Respectively, they yield the compactness and the general shape of the peptide. The radius of gyration is defined as

$$r_g = \frac{\sum_{i=1}^{n} r_i^2}{n+1} \tag{3}$$

where $n$ is the number of atoms and $r_i$ is the distance of each atom from the center of mass of the peptide. A smaller $r_g$ corresponds to a more compact, folded, structure. The asymmetry parameter is defined as

$$\kappa = \frac{2A - B - C}{B - C} \tag{4}$$

where $A$, $B$, and $C$ are the rotational constants of the peptide. The asymmetry parameter ranges from $-1$ to 1 and describes prolate and oblate symmetric top rotors, respectively. These two parameters allow for a fast and semiquantitative means to determine structure.

The H-SAM potential used in this work has been described in detail previously,[42,53−55] and therefore only a brief overview is presented. The potential was developed by Klein and co-workers[53] and consists of both bonded and nonbonded terms. Each chain contains one sulfur atom, $n$ $CH_2$ groups, and one $CH_3$ group. At 0 K, all C atoms are coplanar. The bonded terms in a given chain include harmonic stretches and bends as well as torsional terms. Two types of nonbonded terms are included. The first are nearest neighbor interchain interactions and consist of Lennard-Jones and Buckingham terms. The second are intrachain nonbonded terms between atoms separated by four or more $CH_3$, $CH_2$, or S moieties. Each chain is attached with harmonic stretching terms to three gold atoms. The treatment of the gold layer has been previously shown to be unimportant for energy transfer,[56] and in this work it remains fixed.

The H-SAM unit cell, in this work, consists of $9 \times 9$ $S(CH_2)_7CH_3$ chains arranged into a rhombic lattice with each S atom separated by 4.99 Å, yielding a total of 2349 atoms. Two-dimensional periodic boundary conditions are applied to the H-SAM chains. Automatic construction of the equilibrium geometry and MM force field for the H-SAM was implemented in VENUS[57,58] to facilitate this and future simulations. The interaction potential between protonated peptides and the H-SAM is defined through use of pairwise generalized repulsion terms between individual atoms. The parameters for these terms have been previously determined by Hase and co-workers.[42]

**2.2. The Dynamics.** The classical trajectory simulations were carried out with the general chemical dynamics package, VENUS[57,58] coupled to MOPAC7.0.[59] Initial conditions were selected in which the center of a "beam" of $gly_8$-$H^+$ was aimed at the center of the surface with a fixed incident angle $\theta_i$ with respect to the surface normal and fixed initial collision energy $E_i$.[43] The $gly_8$-$H^+$ ion was randomly orientated with the constraint that its center of mass is centered in the beam and an initial separation of 35 Å from the H-SAM surface. An initial rotational and vibrational temperature of 300 K was assigned to the peptide ion.[60]

A molecular dynamics simulation algorithm was used to select initial conditions for the H-SAM. The steps of the algorithm are as follows. First atomic velocities are assigned by sampling the 300

(49) Bolton, K.; Hase, W. L.; Peslherbe, G. H. In *Modern Methods for Multidimensional Dynamics Computations in Chemistry*; Thompson, D. L. , Ed.; World Scientific: Singapore, River Edge, NJ, 1998; p 143
(50) Sun, L.; Hase, W. L. *Rev. Comput. Chem.* **2003**, *19*, 79.
(51) Hudgins, R. R.; Jarrold, M. F. *J. Phys. Chem. B* **2000**, *104*, 2154.
(52) Wilson, E. B., Jr.; Decius, J. C.; Cross, P. C. *Molecular Vibrations*; Dover Publications Inc.: New York, 1955; p 362.
(53) Hautman, J.; Klein, M. L. *J. Chem. Phys.* **1989**, 4994–5001.
(54) Tasic, U. S.; Yan, T.; Hase, W. L. *J. Phys. Chem. B* **2006**, *110*, 11863–11877.
(55) Tasic, U.; Day, B. S.; Yan, T.; Morris, J. R.; Hase, W. L. *J. Phys. Chem. C* **2008**, *112*, 476–490.
(56) Yan, T.; Hase, W. L. *J. Phys. Chem. B* **2002**, *106*, 8029–8037.
(57) Hu, X.; Hase, W. L.; Pirraglia, T. *J. Comput. Chem.* **1991**, *12*, 1014–1024.
(58) Hase, W. L.; Duchovic, R. J.; Hu, X.; Komornicki, A.; Lim, K. F.; Lu, D. H.; Peslherbe, G. H.; Swamy, K. N.; Vande Linde, S. R.; Zhu, L.; Varandas, A.; Wang, H.; Wolf, R. J. *QCPE Bull.* **1996**, *16*, 671.
(59) A GPL program freely available from http://www.openmopac.net.
(60) Peslherbe, G. H.; Wang, H.; Hase, W. L. *Adv. Chem. Phys.* **1999**, *105*, 171–201.

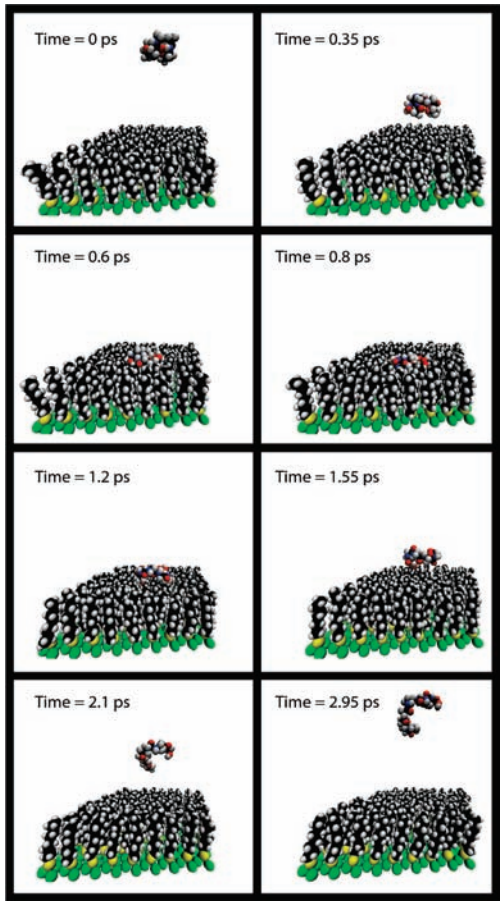


***Figure 2.*** Snap-shots of a trajectory with a collision energy of 90 eV which illustrates the unfolding process. The final radius of gyration and asymmetry parameters are 5.6 and −0.78 respectively.

K Maxwell−Boltzmann distribution. Next an MD simulation is run for 1 ps with velocity rescaling every 0.2 fs followed by an additional 1 ps run without velocity rescaling to ensure equilibration. These final positions and momentum are used as the initial configuration for the trajectory simulation. This approach is used for each trajectory. A sixth order sympletic integration algorithm[61,62] was used to propagate each trajectory with a time step of 1 fs. For each semiempirical method, 320 trajectories were calculated for a range of collision energies, $E_i$, from 5 to 110 eV with $\theta_i = 0°$ and 45°. Trajectories were calculated on the Ranger computer cluster located at the Texas Advanced Computing Center and the Grendel computer cluster located at Texas Tech University. Each individual trajectory, running in serial, required ~3.5 h of wall clock time to complete. Energy was conserved to within at least ±1% of the collision energy for the total simulation time 8.0 ps.

## 3. Trajectory Results

In general the results obtained in this study are consistent with previous calculations[42] and experimental measurements.[12] Snap shots of an example trajectory are displayed in Figure 2. It is apparent from these images that the collision of $gly_8$-$H^+$ with an H-SAM involves a significant interaction and at times a distortion of the H-SAM surface, as well as a change in the final structure of the peptide. Energy transfer to $gly_8$-$H^+$, the H-SAM surface, the final conformation of the peptide, and its fragmentation are examined.

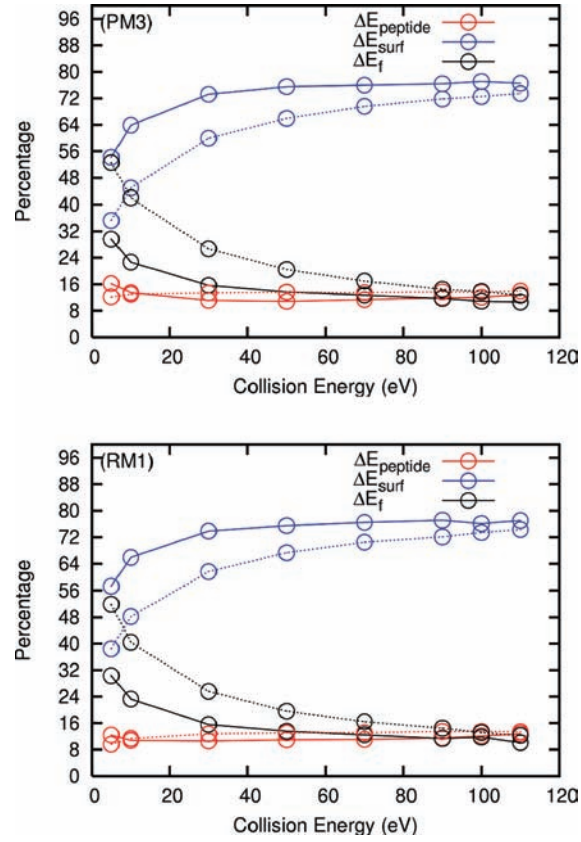


***Figure 3.*** $P_{peptide}(E_i)$, $P_{surf}(E_i)$, and $P(E_f)$ curves for both the RM1 and PM3 simulations. The standard deviation uncertainties range from 0.07 to 0.01. Solid lines give results from the $\theta_i = 0°$ simulations, while dotted lines give $\theta_i = 45°$.

**3.1. Energy Transfer.** During a $gly_8$-$H^+$ + H-SAM collision a significant rearrangement of energy takes place. In Figure 3 the percentage change in internal energy of $gly_8$-$H^+$, $\Delta E_{peptide}$, the H-SAM, $\Delta E_{surf}$, and the final translational energy of $gly_8$-$H^+$, $E_f$, are given. The latter is determined from the conservation relation in eq 1. It is seen that the PM3 and RM1 methods show very close agreement as far as energy transfer percentages are concerned. Therefore, for simplicity of presentation, all of the following figures only display PM3 results. Any dramatic differences between the PM3 and RM1 results will be explicitly stated. The percentage change of internal energy of $gly_8$-$H^+$ is seen to be rather constant with respect to the collision energy, in agreement with previous work.[35] Also in agreement with previous work,[34,35,39] slightly more energy is transferred to $gly_8$-$H^+$ for $\theta_i = 45°$ than 0°. The internal energy of the H-SAM reaches its apparent high-energy asymptote at a lower collision energy for $\theta_i = 0°$ than for $\theta_i = 45°$. As found previously,[39,42,45] the percentage energy transfer to the surface increases and the percentage remaining in final translation decreases, with increase in collision energy.

In a previous study, involving the F-SAM surface,[35] the percentage of energy transferred to internal energy of the surface has been fit to a model based on the adiabaticity[63] parameter and $V \rightarrow T$ energy transfer. It was found that a more physically realistic fit was obtained if the adiabaticity parameter was modified to use the collision energy rather than the velocity,

(61) Schlier, C.; Seiter, A. *J. Phys. Chem. A* **1998**, *102*, 9399.
(62) Schlier, C.; Seiter, A. *Comput. Phys. Commun.* **2000**, *130*, 176.
(63) Levine, R. D.; Bernstein, R. B. *Molecular Reaction Dynamics and Chemical Reactivity*; Oxford: New York, 1987.

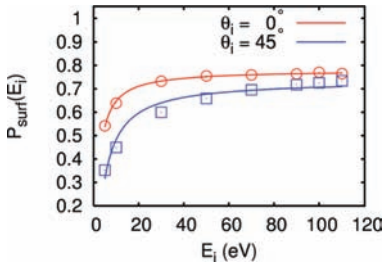


***Figure 4.*** $P_{surf}(E_i)$ curves showing the fit (solid lines) and data (symbols). The parameters $P_0 = 0.781 \pm 0.002$, $b = 1.872 \pm 0.046$ and $P_0 = 0.737 \pm 0.002$, $b = 4.229 \pm 0.442$ for $\theta_i = 0°$ and 45°, respectively. Different asymptotic limits are found for $\theta_i = 0°$ and 45°.

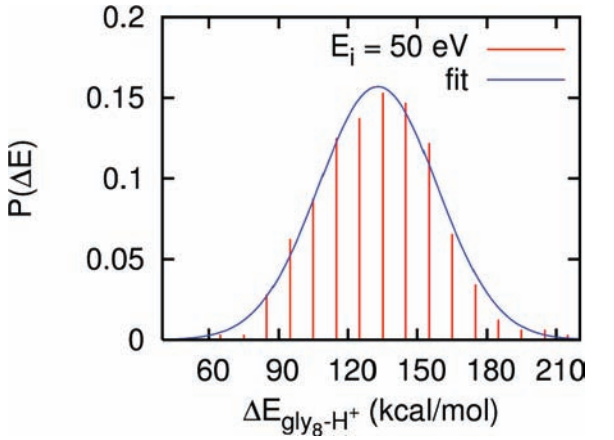


***Figure 5.*** An example comparison of the fits of the internal energy distributions to Gaussian functions. The above distribution is for the internal energy of $gly_8$-$H^+$ with $E_i = 50$ eV and $\theta_i = 0°$.

which we have adopted here. The model for the percentage of energy transferred to the surface is given by

$$P_{surf}(E_i) = \frac{\langle \Delta E_{surf} \rangle}{E_i} = P_0 \exp(-b/E_i) \quad (5)$$

where $\langle \Delta E_{surf} \rangle$ is the average vibrational energy transferred to the surface, while $P_0$ and $b$ are fit parameters. Our results are well fit to such a form, as shown in Figure 4. It is interesting to note that, while the energy transfer to the peptide is more efficient for $\theta_i = 45°$, the converse is true for energy transfer to the surface as shown in Figure 3. A more complete analysis of the data from the above-mentioned F-SAM study is in progress. Preliminary results, which are more accurate than those previously reported, yield $P_0$ values for the F-SAM of 0.85 and 0.72 for $\theta_i = 0°$ and 45°, respectively. In the present work, we obtain values of 0.781 and 0.731, which are quite comparable.

For each collision energy and incident angle there is a distribution of changes in internal energy for both $gly_8$-$H^+$ and the H-SAM, with the mean energy transfer being one measure of these distributions. To quantify these distributions, bins with a 10 kcal/mol width (5 kcal/mol for $E_i = 5$ eV) were constructed for each $E_i$ and $\theta_i$ combination. Each distribution was then fit to a Gaussian of the form,

$$f(E) = Ae^{-(E - E_0)^2/2\sigma^2} \quad (6)$$

which allows for the simple evaluation of the full width at half-maximum (fwhm) and the energy center, $E_0$, for each distribution. An example of the resulting fit is shown in Figure 5. Plots of the fwhm and $E_0$ are given in Figure 6. A linear regression

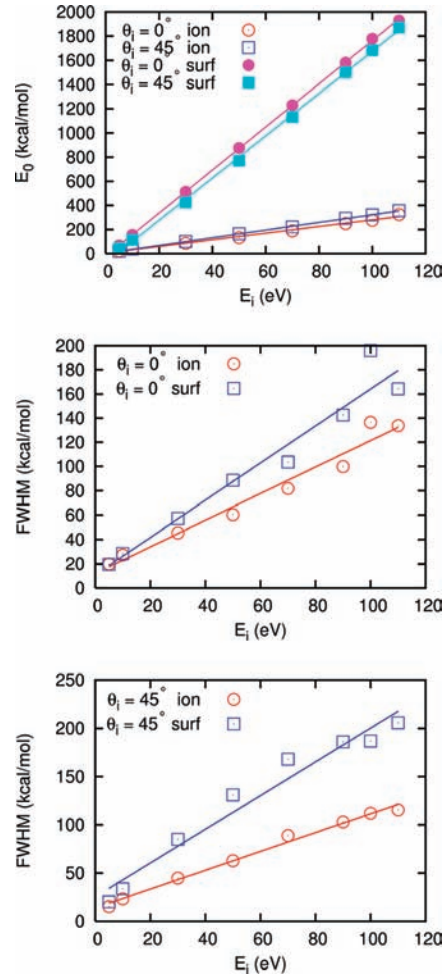


***Figure 6.*** Plots of the centers, $E_0$, and the fwhm of the fits to the internal energy distributions for both $gly_8$-$H^+$ and the H-SAM as a function of collision energy, $E_i$ using PM3. Solid lines represent linear regressions of the values with parameters defined in Table 1. RM1 fits are of similar quality.

***Table 1.*** Fit Parameters and $R^2$ Values for the Distribution Centers and fwhm

| parameter | slope | intercept | $R^2$ |
|---|---|---|---|
| $\theta_i = 0°$ | | | |
| $E_0(gly_8\text{-}H^+)$ | 2.752 (2.740)[a] | 4.9031 (1.526) | 0.994 (0.996) |
| $E_0$(H-SAM) | 17.844 (17.900) | −21.013 (−19.021) | 0.999 (0.999) |
| fwhm($gly_8$-$H^+$) | 1.090 (1.116) | 12.074 (10.826) | 0.968 (0.994) |
| fwhm(H-SAM) | 1.528 (1.593) | 11.007 (8.632) | 0.948 (0.973) |
| $\theta_i = 45°$ | | | |
| $E_0(gly_8\text{-}H^+)$ | 3.171 (3.084) | 4.800 (3.757) | 0.999 (0.999) |
| $E_0$(H-SAM) | 17.478 (17.555) | −72.842 (−66.304) | 0.999 (0.999) |
| fwhm($gly_8$-$H^+$) | 0.973 (1.046) | 13.926 (12.476) | 0.980 (0.991) |
| fwhm(H-SAM) | 1.744 (1.727) | 25.443 (20.499) | 0.962 (0.992) |

[a] RM1 results in parentheses.

of these values yields the slopes and intercepts given in Table 1 which also displays the coefficient of determination, $R^2$. It is seen that the worst of these fits has an $R^2$ value of around 0.948, which shows that the parameters for the distribution are extremely well described by a linear function.

The fwhm of each distribution also show a strong linear dependence, though there is slightly more variation. There is more of a dependence on the bin size for the width of a distribution than for its center. The relatively small number of trajectories calculated also contributes to the statistical "noise."

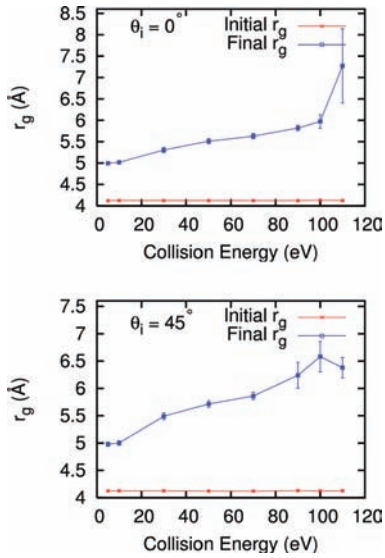


***Figure 7.*** Average radius of gyration, $r_g$, as a function of collision energy for $\theta_i = 0°$ and 45° for the PM3 calculations. Fragmentation effects are seen for $\theta_i = 0°$ and $E_i = 110$ eV.

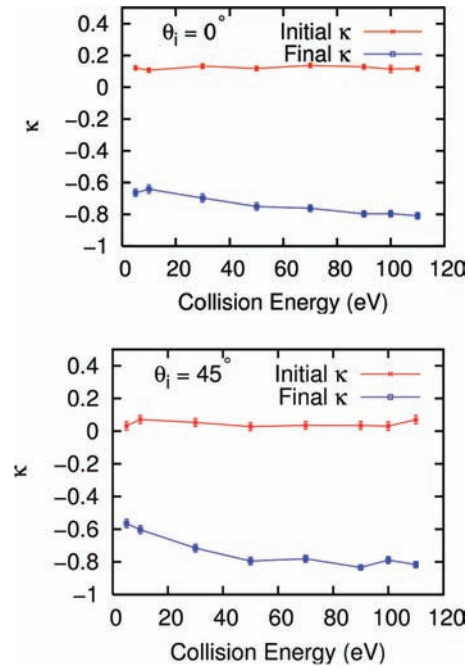


***Figure 8.*** The average asymmetry parameter, $\kappa$, as a function of collision energy for $\theta_i = 0°$ and 45° for the PM3 calculations.

Such effects combine to result in larger errors in fitting the widths, however the fits are still quite good. In general it is seen that the fwhm of the distributions increases with energy, as does the uncertainty in the fit. The $gly_8$-$H^+$ fwhm is always smaller than that for the H-SAM. With a linear fit for both $E_0$ and the fwhm one can predict the energy distribution, in the absence of fragmentation, for a given collision energy.

**3.2. Collision Effects on $gly_8$-$H^+$ Structure.** During the course of the trajectory, energy transfer is not the sole effect. As seen in Figure 2, the final structure of $gly_8$-$H^+$ has undergone a dramatic change, while the H-SAM appears to have recovered a structure similar to that of its initial state. The $gly_8$-$H^+$ ion is initially in a folded structure stabilized by hydrogen bonds. A measure of the compactness of the structure is given by its radius of gyration, which is plotted as a function of $E_i$ in Figure 7 for both the initial and final configurations of $gly_8$-$H^+$. As expected, the initial radius of gyration for $gly_8$-$H^+$ is roughly constant for all $E_i$ and $\theta_i$, since the selection of initial conditions for $gly_8$-$H^+$ is the same for each $E_i$ and $\theta_i$. The only displacement from the equilibrium structure, at this point in the simulation, is due to the 300 K distribution of internal vibrational energy. Following the collision event, the final radius of gyration is significantly larger and increases with increasing collision energy. Differences are seen between $\theta_i = 0°$ and 45°, with the latter resulting in less compact structures. These plots show that on average the final structure of $gly_8$-$H^+$ is less compact than the initial structure, yet it does not give information concerning the relative shape of the peptide. For such insight we turn to the asymmetry parameter.

The asymmetry parameter varies from −1 to 1, describing prolate (cigar-shaped) or oblate (frisbee-shaped) molecules, respectively. Plots of the asymmetry parameter as a function of the collision energy are shown in Figure 8. It should be noted that this parameter is defined using the rotational constants, which for $gly_8$-$H^+$ are relatively small. Therefore, small changes can result in large changes in the asymmetry parameter. Despite this caveat, this parameter does yield a simple and qualitative measure of average changes in the structural shape of $gly_8$-$H^+$. This is justified by examining the initial average value of $\kappa$ in Figure 8. A 300 K rotational and vibrational distribution does not result in large deviations in $\kappa$. In contrast, as seen from the final value, collisions have a significant effect on the asymmetry parameter. A strong preference is found toward prolate shaped molecules following the collision. This shows that collisions of a folded peptide with an H-SAM results in unfolded peptides which tend to be straight-chain-like.

Through examining Figures 6 and 7 it is seen that the conformational changes are larger for an incident angle of 45°. One possible explanation involves the fundamental difference between the two incident angles. In the normal incident case, all of the kinetic energy is directed straight into the surface which may actually result in a squished peptide as an intermediate structure. However, for the 45° case a tumbling or a frictional drag like effect on the peptide is possible and appears to assist in the unfolding process. These conformational changes are the low-energy/short-time analogue of fragmentation.

**3.3. Intramolecular Proton Transfer and Fragmentation of $gly_8$-$H^+$.** No shattering fragmentations are observed in the simulations. However, after $gly_8$-$H^+$ has unfolded, in some of the trajectories, there is fragmentation promoted by intramolecular proton transfer. The proton transfer and fragmentation dynamics are very similar for 0° and 45° incident angles, and occur in both the PM3 and RM1 simulations, with similar atomic-level dynamics. However, the probabilities are much higher for the RM1 simulations. To illustrate, for $E_i = 100$ eV with either incident angle, proton transfer occurs in 62% of the RM1 trajectories but in only 14% of the PM3 trajectories. Hence, the RM1 results are used for the statistical analysis below. Of all the hydrogen atoms in $gly_8$-$H^+$ the ones located on the terminal, protonated nitrogen are most likely to be involved in the proton transfer. It is of no surprise that these hydrogen atoms are the most likely to migrate, since they carry most of the ion's positive charge. The most probable receptor site for these proton migrations are the nitrogen and oxygen of the first peptide bond. For $E_i = 110$ eV these sites account for 61% and 66%, for $\theta_i = 0°$ and 45°, respectively, of the proton transfers from the terminal nitrogen for the RM1 simulations.

The oxygen and nitrogen involved in peptide bonds further down the chain are the next most likely proton transfer sites with the percentages decreasing with distance from the terminal nitrogen site, e.g. the probability of proton transfer to the second peptide bond is a factor 6 smaller than proton transfer to the first peptide bond. The proton transfers take place after the peptide has unfolded, and hence the nitrogen and oxygen atoms closest to the terminal nitrogen are the most likely receptor sites. There is a very small probability, i.e. 1%, for proton transfer to the carbonyl C-atom closest to the $-NH_3^+$ group.

It is known that proton transfer is an important step in the fragmentation process,[64] and this property is observed here. For the RM1 simulations at $E_i = 110$ eV and $\theta_i = 0°$, proton transfer plus fragmentation occurs in 45% of the trajectories, proton transfer alone in 14%, and fragmentation alone in 0.6%. These percentages are 52%, 13%, and 2.5% for $\theta_i = 45°$. These results are for the 8 ps trajectories, and the percentages are expected to increase if the dynamics are studied for a longer period of time. However, they illustrate the importance of proton transfer in promoting fragmentation. The large difference in the proton transfer probabilities for the PM3 and RM1 simulations leads to large differences in their fragmentation probabilities. For the $\theta_i = 0°$ PM3 simulations there are no fragmentations for collision energies of 90 eV or less, with 9% and 6% of trajectories fragmenting at $E_i = 100$ and 110 eV, respectively. Using RM1 for $\theta_i = 0°$ there are no fragmentations at $E_i = 5$ and 10 eV, with 0.6, 4, 9, 23, 32, and 46% of the trajectories fragmenting at 30, 50, 70, 90, 100, and 110 eV, respectively. Though the $gly_8$-$H^+$ ions fragmenting at a specific $E_i$ have a range of internal energies, the number of $gly_8$-$H^+$ ions surviving versus time is approximately exponential. Thus, approximate unimolecular lifetimes, $\tau$, may be obtained from plots of ln[$gly_8$-$H^+$ ] versus time. For the RM1 simulations at $\theta_i = 0°$ the resulting $\tau$ are 12, 19, 31, 93, and 220 ps for $E_i$ of 110, 100, 90, 70, and 50 eV, respectively.

Although the fragmentation time scales and percentages are different between the PM3 and RM1 methods, the major fragmentation pathways observed are the same. For our analysis of the fragmentation pathways we adopt a similar notation to that used for ion fragments in mass spectrometry studies.[65] However, we use the notation only to identify the sites for which bond breakage has occurred. We find that by far the most probable pathways consist of either a single A−X bond breakage or coincident A−X and B−Y bond breakage. A−X denotes $CH_2$ −CO bond breakage, while B−Y is breakage of the a peptide bond.

## 4. Comparisons with Previous Studies

**4.1. Experiment.** The current results may be compared with the experimental work of Laskin and Futrell.[12] Their experiment consists of the collision of the singly protonated octa-peptide des-Arg[1]-bradykinin with several surfaces, including an H-SAM. Although this peptide is structurally different than $gly_8$-$H^+$ these chemical details may be unimportant, insofar as the average energy transfer is concerned, since these collisions are assumed to be in the impulsive regime.[35,39,45] Both qualitative agreement (cf. Figures 4 and 6 of Laskin and Futrell[12]) and quantitative agreement is found with their results. They derive an average energy transfer to the octa-peptide, based on their linear regression, of 10.1 ± 0.8%. Using the same approach, our average energy transfer to $gly_8$-$H^+$ is 11.9%, which is quite close to the experimental value. Note that this value is a better measure of the computational energy transfer percentage than any single given value in Figure 3 as it makes use of all 2560 trajectories calculated for normal incidence. At $\theta_i = 45°$ our average energy transfer is 13.8% and 13.4% for the PM3 and RM1 models respectively. Our percentage of energy transferred to the projectile peptide is also very similar to that seen by Cooks[66] and Wysocki[67] in collisions of hydrocarbon projectiles with an H-SAM. In comparing our distribution widths we again see qualitative agreement though our actual number is larger by nearly a factor of 2 than the value obtained from the experimental distributions, which were determined by a RRKM analysis. Similar explanations as to those discussed above, concerning the fitting of the fwhm for a simulation's distribution of change in internal energy, provide one explanation as to why the precise number is different between simulations and experiment. It is also possible that, though the same average percentage energy is transferred to $gly_8$-$H^+$ and des-Arg[1]-bradykinin, there may be a difference in the widths of their energy transfer distributions.

One aspect of experiment which is missed in our simulations is the fragmentation efficiency. Fragmentation of $gly_8$-$H^+$ is observed in the 8 ps simulation reported here and at the highest collision energy of 110 eV 6% and 46% of the PM3 and RM1 trajectories, respectively, fragment. The collisions impart a significant amount of vibrational energy to the peptide and more fragmentation is expected at all collision energies if the trajectories were integrated for a longer period of time. Using the internal energy distributions of $gly_8$-$H^+$ and RRKM theory the fragmentation efficiency at each collision energy could be determined if the fragmentation pathways and their activation energies and frequency factors were known.[14,68] However, obtaining this information either experimentally[14,68] or computationally is a challenging problem. For a 60 eV collision energy a fragmentation efficiency of 50% is observed in the des-Arg[1]-bradykinin + H-SAM experiments.[12] In comparison, for the $gly_8$-$H^+$ + H-SAM simulations there is no fragmentation at $E_i = 60$ eV when using PM3 and 4% at $E_i = 50$ eV, and 9% at $E_i = 70$ eV when using RM1. As discussed above, more fragmentation is expected if the dynamics is followed for a longer time than the 8 ps of the trajectories. Nevertheless, the fragmentation dynamics of $gly_8$-$H^+$ and des-Arg[1]-bradykinin may differ. For $gly_8$-$H^+$ there is no shattering and fragmentation occurs after $gly_8$-$H^+$ has unfolded. Fragmentation is promoted by proton transfer from the terminal $NH_3^+$ group to atoms with the first glycine unit. Shattering fragmentation has been inferred for bradykinin,[12] which occurs before the peptide unfolds. Proton transfer pathways for folded bradykinin may be substantially different than what is found here for unfolded $gly_8$-$H^+$. Also, the series of amino acids for bradykinin may have their own unique fragmentation patterns.

**4.2. Chemical Dynamics Simulations.** The results of the current simulation of $gly_8$-$H^+$ + H-SAM collisions are quite consistent with a previous simulation of $gly_3$-$H^+$ + H-SAM collisions.[42] For this earlier study, with the folded $gly_3$-$H^+$

(64) Dongré, A. R.; Jones, J. L.; Somogyi, Á.; Wysocki, V. H. *J. Am. Chem. Soc.* **1996**, *118*, 8365.
(65) Papayannopoulos, I. A. *Mass. Spectrom. Rev.* **1995**, *14*, 49.
(66) Grill, V.; Shen, J.; Evans, C.; Cooks, R. G. *Rev. Sci. Instrum.* **2001**, *72*, 3149–3179.
(67) Vékey, K.; Somogyi, A.; Wysocki, V. H. *J. Mass. Spectrom.* **1995**, *30*, 212.
(68) Laskin, J. In *Principles of Mass Spectrometry Applied to Biomolecules*; Laskin, J. , Litshitz, C. , Eds.; Wiley: Hoboken, NJ, 2006; p 619

structure, the percentage energy transfer to $\Delta E_{peptide}$ and $\Delta E_{surf}$ are 7% and 63% with 30% remaining in $E_f$, for collisions with $E_i = 30$ eV and $\theta_i = 45°$. In comparison to the current gly$_8$-H$^+$ + H-SAM simulation (Figure 3), the principal differences for gly$_3$-H$^+$ + H-SAM are a smaller percentage transfer to $\Delta E_{peptide}$ and larger percentage remaining in $E_f$. However, overall, these differences are quite small. It is of interest that the average energy transfer percentages for the above peptide-H$^+$ + H-SAM collisions are similar to those found from a simulation of $Cr^+(CO)_6$ + H-SAM collisions at the same $E_i$ and $\theta_i$.[41,43] For this latter system, the average percentages in $\Delta E_{peptide}$, $\Delta E_{surf}$, and $E_f$ are 10%, 69%, and 21%, respectively. The relative insensitivity of the energy transfer efficiencies to detailed properties of the projectile, for collisions with SAM surfaces, has been pointed out and discussed previously.[42]

Chemical dynamics simulations of gly$_8$-H$^+$ with a diamond surface have been performed.[34] Unlike the present study, shattering trajectories are prevalent for a collision energy of 100 eV with 78% and 22% of the trajectories shattering at incident angles of 0° and 45°, respectively. The presence or absence of shattering trajectories is expected to be closely related to the properties of the surface, specifically the "stiffness" of the surface. Diamond and H-SAM surfaces represent opposite extremes, with diamond being quite stiff. If trajectories had been performed for a fluorinated hydrocarbon surface, shattering trajectories would likely be seen as the F-SAM is significantly stiffer than the H-SAM.[35] Shattering has been observed and quantified in experimental studies of isomers of des-Arg$^1$-bradykinin colliding with a F-SAM surface.[14,15] It is noteworthy that shattering has been suggested for collisions of des-Arg$^1$-bradykinin with a H-SAM,[12] and this experimental result, as compared to the absence of shattering found here for gly$_8$-H$^+$ + H-SAM collisions, needs additional study. Peptide-H$^+$ fragmentation pathways have been characterized in previous simulations of gly-H$^+$,[46] gly$_2$-H$^+$,[40] and gly$_8$-H$^+$[36] colliding with the diamond {111} surface. The dominant fragmentation pathways found in these simulations are A−X and B−Y cleavages as found here for gly$_8$-H$^+$ + H-SAM collisions. However, for gly$_8$-H$^+$ + diamond {1 1 1} SID[36] $NH_3^+$ $-CH_2$ bond cleavage is also important.

The percentage energy transfer to the peptide ion's internal degrees of freedom is nearly independent of the collision energy. In contrast, the percentage energy transfer to the surface vibrational modes increases with collision energy to an apparent asymptotic value. These effects have been seen and discussed for previous simulations.[39,42,45] An effect not studied in previous simulations of peptide-H$^+$ + H-SAM collisions is the dependence of the energy transfer efficiencies on the incident angle. For the gly$_8$-H$^+$ + H-SAM collisions the percentage transfer to $\Delta E_{peptide}$ is nearly independent of 0° and 45° incident angles, with a slightly higher percentage at 45°. In contrast, changing $\theta_i$ from 0° to 45° increases energy transfer to $\Delta E_{surf}$ These different effects of $\theta_i$ on energy transfer to $\Delta E_{peptide}$ and $\Delta E_{surf}$ are particularly interesting.

In previous experimental studies of projectile ion collisions,[11,69] with SAM and a liquid hydrocarbon surfaces, it was found that the percentage energy transfer to the projectile's internal degrees of freedom is nearly independent of the incident angle; i.e. the result found here for gly$_8$-H$^+$ + H-SAM collisions. In contrast, energy transfer to $\Delta E_{peptide}$ for gly$_8$-H$^+$ + diamond {1 1 1} collisions is strongly dependent on $\theta_i$.[36] For $E_i = 100$ eV collisions, the percentage transfer to $\Delta E_{peptide}$ is 45% and 26% for $\theta_i$ of 0° an 45°, respectively.[36] Though a definitive answer is not possible for the different energy transfers to $\Delta E_{peptide}$ for gly$_8$-H$^+$ collisions with the H-SAM and diamond {1 1 1} surfaces, it is useful to review the strikingly different properties of these two surfaces. Compared to the H-SAM, diamond {1 1 1} is a smooth, rigid surface (see detailed discussion below). The H-SAM is a soft, highly corrugated surface, with substantial roughness[70,71] As a result, the 0° and 45° incident angles may have similar dynamics for energy transfer to $\Delta E_{peptide}$. Previous simulations have shown that the $\Delta E_{peptide}$ energy transfer is primarily to the peptide ion's dihedral degrees of freedom[42] and apparently this is the same for 0° and 45°. It is noteworthy, that for Ne + H-SAM collisions the same energy transfer efficiencies are seen at 0° and 45°.[72]

For a smooth rigid surface the energy transfer only depends on the normal component of the incident energy and scales by $E_i \cos^2 \theta_i$.[70−72] The gly$_8$-H$^+$ + diamond {1 1 1} collisions at $E_i = 100$ eV conform to these dynamics.[36] The percentage energy transfer to $\Delta E_{peptide}$, $\Delta E_{surf}$, and $E_f$ are 45, 26, and 29% at $\theta_i = 0°$. For $\theta_i = 45°$ these percentages are 26, 12, and 62%, respectively, and are approximately a factor of 2 different than the $\theta_i = 0°$ values, consistent with the $\cos^2 \theta_i$ scaling. As shown by the energy transfer percentages in Figure 3 such scaling is not present for the gly$_8$-H$^+$ + H-SAM energy transfer.

## 5. Summary

We have presented results from PM3 and RM1 direct dynamics simulations of the gly$_8$-H$^+$ + H-SAM collision system. Trajectories were calculated for a range of collision energies from 5−110 eV with incident angles of 0 and 45°. Our results are in excellent agreement with previous computational and experimental work, with our average energy transfer at normal incidences falling within 2% of experimental results.[12]

The PM3 (RM1) percentage energy transfer to the gly$_8$-H$^+$ internal degrees of freedom, independent of the collision energy, are 11.9% (11.9%) and 13.8% (13.4%) for incident angles of 0° and 45°, respectively. In experimental studies of des-Arg$^1$-bradykinin + H-SAM collisions,[12] the percentage energy transfer to the octapeptide is found to be 10.1 ± 0.8%, similar to our results for gly$_8$-H$^+$. Our distribution widths are in qualitative agreement with the experiments for des-Arg$^1$-bradykinin. Strong linear relations between the centers and fwhm of the internal energy distributions are seen, again in good agreement with experimental results. Although energy transfer to the peptide is more efficient at 45° the opposite is true for transfer to the H-SAM; e.g., with the PM3 potential, the energy transfer efficiencies are 76.5% and 73.4% for 0° and 45°, respectively, at the 110 eV collision energy. In agreement with previous simulations,[41−43] the percentage energy transfer to the surface increases with the collision energy.

Conformational effects due to the collision are observed. The initial state of the gly$_8$-H$^+$ molecule is that of a folded peptide chain. Through an examination of the radius of gyration and the asymmetry parameter we show that after the collision there is a strong propensity toward a straight-chain structure. These observations show that one could prepare a straight-chain peptide with a well-defined internal energy distribution through collisions with H-SAM surfaces in the absence of fragmentation.

(69) Žabka, J.; Dolejšek, Z.; Herman, Z. *J. Phys. Chem. A* **2002**, *106*, 10861.
(70) Tully, J. C. *J. Chem. Phys.* **1990**, *92*, 680.
(71) Yan, T.; Hase, W. L.; Tully, J. C. *J. Chem. Phys.* **2004**, *120*, 1031.
(72) Yan, T.; Hase, W. L. *Phys. Chem. Chem. Phys.* **2000**, *2*, 901.

Fragmentation does occur within the 8 ps simulation time, but only at high collision energies. The RM1 semiempirical model for the $gly_8$-$H^+$ intramolecular potential gives substantially more fragmentation than does the PM3 model. Fragmentation occurs after the peptide ion has unfolded and there are no shattering events[14−16,34,36,40,41,46] leading to fragmentation. A substantial amount of energy is transferred to $gly_8$-$H^+$ and more fragmentation is expected if the dynamics are followed for longer times. If information were available concerning energies, structures, and vibrational frequencies for fragmentation transition states (TSs),[68,73] RRKM theory calculations could be combined with the $gly_8$-$H^+$ internal energy distribution determined from the simulations to calculate the fragmentation efficiency. A direct comparison with experiment[12,13] could then be made. Unfortunately, such TS information is unavailable for $gly_8$-$H^+$ fragmentation, and its determination is an important issue for future studies.

(73) Laskin, J.; Bailey, T. H.; Denisov, E. V.; Futrell, J. H. *J. Phys. Chem. A* **2002**, *106*, 9832.

In this work we have examined collisions between a peptide ion and an H-SAM surface in the impulsive regime. However, it would be of great interest to perform a simulation in which reactive chemistry is possible. Experimentally it is seen that reactive landing occurs and depends on both the chemical nature of the peptide and the SAM headgroup.[5] The current treatment of the H-SAM potential, as an MM force field, precludes chemical reaction between the surface and the peptide. In future work we plan to create a QM/MM model in which a portion of the surface is included in the QM region. This would allow for full chemical reactivity.

**Acknowledgment.** This material is based upon work supported by the National Science Foundation under Grant Nos. CHE-0615321 and OISE-0730114 and the Robert A. Welch Foundation under Grant No. D-0005. Support was also provided by the High-Performance Computing Center (HPCC) at Texas Tech University, under the direction of Philip W. Smith, as well as the Texas Advanced Computing Center (TACC) at The University of Texas at Austin by providing HPC resources.

JA904925P